# Journal Pre-proof

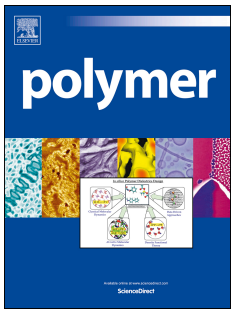


Diaminomaleonitrile as a high-throughput precursor for alternative layered C]N-BASED conjugated polymers to carbon nitrides

Marta Ruiz-Bermejo, Carlos Hortelano, M. Pilar García Armada, José L. de la Fuente

PII: S0032-3861(24)00182-4

DOI: https://doi.org/10.1016/j.polymer.2024.126847

Reference: JPOL 126847

To appear in: *Polymer*

Received Date: 14 November 2023

Revised Date: 19 February 2024

Accepted Date: 26 February 2024

Please cite this article as: Ruiz-Bermejo M, Hortelano C, García Armada MP, de la Fuente JoséL, Diaminomaleonitrile as a high-throughput precursor for alternative layered C]N-BASED conjugated polymers to carbon nitrides, *Polymer* (2024), doi: https://doi.org/10.1016/j.polymer.2024.126847.

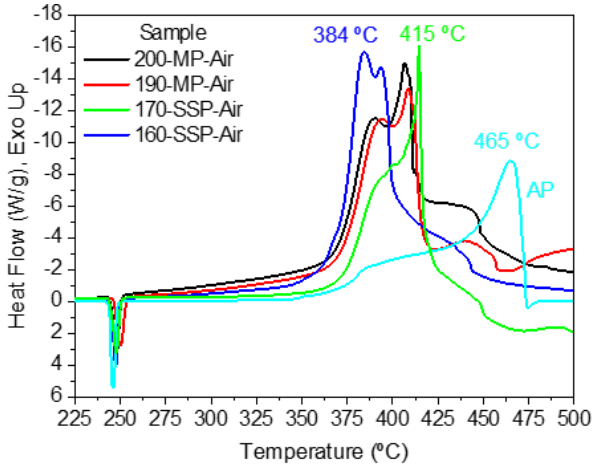


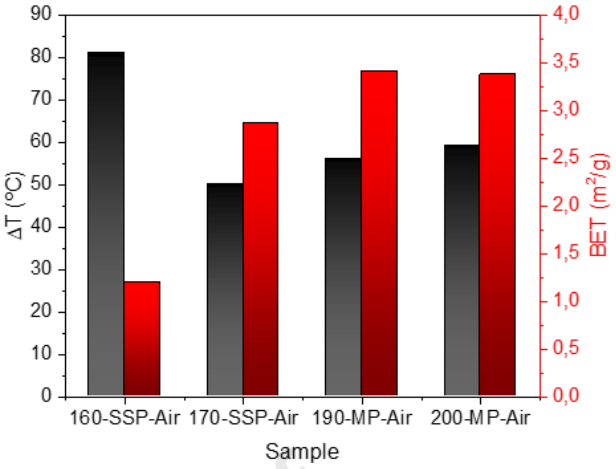


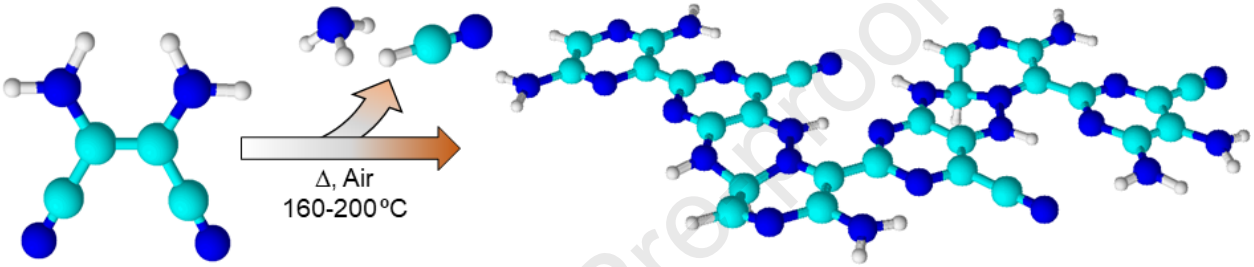

# DIAMINOMALEONITRILE AS A HIGH-THROUGHPUT PRECURSOR FOR ALTERNATIVE LAYERED C=N-BASED CONJUGATED POLYMERS TO CARBON NITRIDES

Marta Ruiz-Bermejo[a], Carlos Hortelano[b], M. Pilar García Armada[c] and José L. de la Fuente[b]*

[a] Centro de Astrobiología (CAB), CSIC-INTA. Ctra. Torrejón-Ajalvir, km 4, Torrejón de Ardoz, 28850 Madrid, Spain.

[b] Instituto Nacional de Técnica Aeroespacial "Esteban Terradas" (INTA). Ctra. Torrejón-Ajalvir, km 4, Torrejón de Ardoz, 28850 Madrid, Spain.

[c] Departamento de Ingeniería Química y Medio Ambiente, Escuela Técnica Superior de Ingenieros Industriales, Universidad Politécnica de Madrid, José Gutiérrez Abascal 2, 28006 Madrid, Spain

*Corresponding author information: email: fuentegj@inta.es

Telephone: 34915201841 Fax: 34915201611

**ABSTRACT**

In the present work, the fast production of C=N-based conjugated macrostructures from the bulk thermal polymerization of diaminomaleonitrile (DAMN) is discussed. These high-throughput syntheses showed air tolerance and were studied under different temperature regimes, from 160 to 200 °C, according to solid-state or melt polymerization (MP). This study displays not only the effect of temperature and exposure to air but also the gases evolved during the polymerization reactions. These volatiles were suitably analysed, providing relevant information about the elimination processes that take place during the course of these thermolytic reactions. The microstructure and physical properties of these black polymer materials obtained were determined by elemental analysis, Fourier transform infrared (FTIR), nuclear magnetic resonance (NMR) and ultraviolet–visible (UV–Vis) spectroscopies, X-ray diffraction (XRD), thermogravimetry (TG), electron paramagnetic resonance (EPR), electrochemistry measurements and scanning electron microscopy (SEM). The interpretation of all these data suggests that a two-dimensional (2-D) macrostructure based on N-heterocycles as diazines is predominant, regardless of the state of monomer aggregation during the course of the polycondensations. Interestingly, these 2-D polymeric systems present characteristic analogues with well-documented carbon nitrides (g-$C_3N_4$), with similar magnetic, electrochemical, optical and catalytic properties. Thus, DAMN polymers are proposed as alternative materials to relevant g-$C_3N_4$, as their synthetic process is easy, quick and highly efficient.

**Keywords**: diaminomaleonitrile; HCN polymers; thermal polymerization; catalysis; bidimensional materials

## 1. INTRODUCTION

Polymeric graphitic carbon nitrides (g-$C_3N_4$) are a wide material family with not only different carbon-to-nitrogen ratios but also diverse basic structural units and linkages, including triazine, triazole, tri-heptazine and azo linkages. Their general formula is near $C_3N_4$, although they are better described as $C_xN_yH_z$, since H is an essential component of their structures. In addition, the different classes of these functional materials generated by various chemical and physical routes, exhibit dissimilar degrees of condensation, properties and reactivity depending on the precursor and the reaction conditions. They are being investigated as potential next-generation materials for incorporation in devices for energy conversion and storage as well as for optoelectronic and catalysis applications [1-3]. Large synthetic strategies have been applied to obtain g-$C_3N_4$ and their films, which can be facilely prepared from precursors such as cyanamide, dicyanamide, urea, melamine and their mixtures [4-6]. In addition to these ordinary organic precursors, biotic compounds, such as nucleobases, have been used to obtain these emerging functional materials, which are usually synthesized by controlled pyrolysis over a wide range of temperatures above 500 °C [7]. They play a key role in the field of solar-fuel conversion and environmental remediation due to their adjustable photoelectric properties, intrinsic earth-abundant nature, environmental friendliness and outstanding physicochemical stability. However, the high temperatures and long reaction times habitually needed in their syntheses together with the relatively low yields found in some processes seriously limit their scaling. On the other hand, their low electronic conductivity, lack of absorption above 460 nm and low surface area in bulk g-$C_3N_4$ hinder some of their applications.

Thus, new precursors and synthetic strategies are continually being explored to overcome the previously argued limitations [8]. In recent years, our research group has begun to explore the relationship between g-$C_3N_4$ and so-called HCN-derived polymers using diaminomaleonitrile (DAMN, the formal tetramer of HCN) as a potential monomer [9-14]. In a first study, the DAMN hydrothermal polymerizations at 80 °C were described, finding truly high yields, approximately 75%, and some structural features that present similarity with conventional g-$C_3N_4$ [9]. Previously, Mamajanov and Herzfeld proved bulk thermal-induced polymerization in the solid-state of crystalline DAMN [15]. They found that moderate heating, 125 °C, under argon indeed results in an unmistakable reaction, with the abrupt transformation of pale crystallites to shrunken dark particles. Moreover, DAMN has been used as a co-monomer together with urea by heating at 500

°C to obtain g-$C_3N_4$ as a low-dimensional organic semiconductor [16]; and novel nitrile polymers based on DAMN continue to arouse interest as high-performance materials [17,18].

These precedents encouraged us to explore in detail the thermal behaviour of DAMN and its potential for the production of macrostructures such as g-$C_3N_4$. The thermal analysis of DAMN was quite revealing, so by means of dynamic differential scanning calorimetry (DSC) analyses, it was discovered that the bulk thermal polymerization of DAMN under an inert nitrogen environment can take place both in the solid and in the molten state [10,11]. From these calorimetric measurements, the kinetic study carried out demonstrated the autocatalytic character of these highly efficient bulk polymerizations, with yields in the range of 85-90%, and corroborated that these thermally induced reactions are extremely fast in a molten state [10,11]. Moreover, polymeric materials based on DAMN, obtained by solid-state polymerization (SSP) or through melt polymerization (MP) under an inert atmosphere, are effective electroactive redox systems that are useful for the development of biosensors [12]. These promising results led to the evaluation of the impact of air on bulk DAMN polymerizations under different temperatures since operating under atmospheric conditions would simplify and reduce the production cost of these novel kinds of C=N-based conjugated materials. Thus, we confirmed by a thermoanalytical technique, such as DSC, the effective air tolerance of the DAMN thermal polymerization [14].

One step beyond, herein, the synthesis of DAMN polymers by bulk thermal polymerization under atmospheric conditions is described at the preparative scale, both in SSPs and in MPs. The structural characteristics of these new series of DAMN-based polymers are compared with those previously described but obtained under a nitrogen atmosphere. In addition, their magnetic, electrochemical and optical properties, together with their catalytic activity for the thermal decomposition of ammonium perchlorate (AP), which is a fundamental component in advanced composite energetic materials, are defined and discussed. As a result, these DAMN polymers were obtained at high yields in very simple and fast processes at moderately high temperatures, and they exhibit a high analogy with g-$C_3N_4$ and even improve some of their performances.

Completing this study and taking into account the environmental restrictions of industrial processes, a new methodology to identify and collect the gases generated during the course of these thermal syntheses was established, which allowed the clarification of

certain mechanistic aspects of DAMN polymerizations. Thus, on the basis of these reactions and the spectroscopic data compiled and analysed here, novel C=N conjugated macrostructures for DAMN polymers are rationally proposed and discussed. In this way, the present work introduces an effective one-pot and low-cost synthetic method for the production of layered $C_xN_yH_z$ materials with potential applications as alternative g-$C_3N_4$.

## 2. Materials and methods

### *2.1.Thermal polymerizations*

DAMN was purchased from Sigma Aldrich (98%) and used as received. Although some thermal polymerizations were conducted by DSC as described below, isothermal polymerization reactions using heated metal blocks were carried out. Thus, two series of experiments were planned. One used 20 ml capped vials with Teflon set-ups (series 1), and the second one was done in an analogous way but using 10 ml vials (totally inside in the holes of the heating-blocks) and balloons inserted in the set-ups as containers to collect the evolve gas during the polymerization reactions (series 2), as shown in **Fig. S1**. Experiments at 190 and 200 °C were conducted to investigate the DAMN MPs, while two temperatures of 160 and 170 °C were applied when the SSPs were analysed. In both cases, the experiments were performed under atmospheric conditions. Series 1 was clarifying and revealing since it allowed visualization of the collateral HCN polymerization during the thermal polycondensation of DAMN, as explained later, and it can be seen in the video collected in the **Supplementary Information**. In a first approach to try to remove the HCN released during the DAMN polymerization, this one was pumped to a cold solution of iron (II) sulfate heptahydrate (**Fig. S2**). In this way, a pure DAMN polymer was obtained in the vial warning in the heating block, and a green–blue suspension was collected after the reaction time in the cold tramp of the sulfate solution. This suspension was centrifuged, and two phases were isolated. The supernatant was freeze-dried, finally leading to a grey–yellow solid. The precipitate was also dried under reduced pressure, and finally, a powered blue solid was obtained. The Fourier transform infrared (FTIR) spectra of both phases indicate the formation of several ferrocyanides (Fig. S2). The spectrum from the supernatant presents bands centred at 2047 and 1410 $cm^{-1}$, which can be related to the formation of $(NH_4)_4[Fe(CN)_6]$. In addition, the IR spectrum of the blue solid precipitate shows features centred at 2069 and 1410 $cm^{-1}$, which can be assigned to the production of $(NH_4)Fe[Fe(CN)_6]$. Both spectra were compared with those of authentic standards of

$(NH_4)_4[Fe(CN)_6]$ and $(NH_4)Fe[Fe(CN)_6]$ synthetized as described in the literature [19], confirming the formation of these ferrocyanides under the synthetic conditions considered here. This device allowed us for the first time to demonstrate that during DAMN polymerization, appreciable amounts of HCN and $NH_3$ are released. Approximately 15% of the mass, or even less depending on the polymerization temperature, is lost by the initial amount of DAMN put in the system, as discussed later. However, to produce pure DAMN polymers but using a simpler synthetic methodology and taking in mind that the gases go from the high to the low pressure zone, balloons were inserted in the vials (series 2) (Fig. S1). Thus, HCN and $NH_3$ were collected in the interior of the balloons (see the final colour of white balloons after the secondary polymerization of liquid HCN inside them, especially in the series carried out at higher temperatures), and pure DAMN polymers were obtained.

Nonisothermal runs were carried out in a Perkin Elmer DSC-7 calibrated with high-purity chemicals. Samples of approximately 10 mg of DAMN, placed in aluminium pans, were dynamically polymerized under 20 ml/min of dry nitrogen and air atmospheres. These scans allowed the selection of suitable temperatures for isothermal polymerization at the preparative scale described above, in accordance with previous studies [10,11,14].

### *2.2. Structural characterization, optical, electrochemical and magnetic properties, and morphological features*

The DAMN polymers were examined to determine the mass fractions of carbon, hydrogen and nitrogen using a Perkin Elmer elemental analyser, model CNHS-2400. The percentages of oxygen in the samples were obtained by calculating the differences. Diffuse reflectance spectra were acquired in the 4000–400 $cm^{-1}$ spectral region using an FTIR spectrometer (Nicolet, model NEXUS 670) configured with a drift reflectance accessory (Harrick, model Praying Mantis DRP) mounted inside the instrument compartment. The spectra were obtained in CsI pellets, and the spectral resolution was 2 $cm^{-1}$. $^{13}C$ solid-state cross polarization/magic angle spinning nuclear magnetic resonance (CP/MAS NMR) spectra were obtained using a Bruker Advance 400 spectrometer and a standard cross-polarization pulse sequence. Samples were spun at 10 kHz, and the spectrometer frequency was set to 100.62 MHz. A contact time of 1 ms and a period between successive accumulations of 5 s were used. The number of scans was 5000, and the chemical shift values were referenced to tetramethylsilane. The thermal degradation

properties of the DAMN polymers were studied using thermogravimetry (TG), DSC and differential thermal analysis (DTA) measurements with an SDTQ-600/Thermo Star simultaneous thermal analyser (TA Instrument). The nonisothermal experiments were carried out under dynamic conditions from room temperature to 1000 °C at a heating rate (β) of 10 °C/min under an argon atmosphere. The average sample weight was ~ 20 mg, and the argon flow rate was 100 ml/min. The ultraviolet–visible diffuse reflectance spectroscopy (UV–Vis DRS) of the samples was measured on an UV–Vis spectrophotometer Jaco Model V-660 using the Kubelka Munk transformation and Tau equation to obtain the apparent band gap. All electrochemical studies were performed with an Ecochemie BV Autolab PGSTAT 12 with a conventional three-electrode cell at 20-21 °C. The electrodes were a Pt disc (3 mm diameter) as the working electrode, a Pt wire as the auxiliary electrode and a saturated calomel electrode (SCE) (E = 0.2412 V vs. SHE) as the reference electrode. All electrochemical measurements were performed in 0.1 M $NaClO_4$ as the supporting electrolyte. To modify the working electrodes, the materials were ground, suspended in absolute ethanol and mixed with the same volume of Nafion (diluted 50% in methanol). The mixtures were sonicated (for 20 min). The working electrodes were prepared by dropping 5 µl of these suspensions on the surface of Pt disc electrodes and letting them dry in air at room temperature. The modified electrodes were used without another pretreatment. Electron paramagnetic resonance (EPR) spectroscopy was carried out at room temperature with a Bruker EMX spectrometer operating at 9.44 GHz (X-band) and using 25 mg of powered sample. Powder X-ray diffraction (XRD) measurements were performed using a Bruker D8 Eco Advance with Cu Kα radiation ($\lambda$ = 1.542 Å) and a Lynxeye XE-T linear detector. The X-ray generator was set to an acceleration voltage of 40 kV and a filament emission of 25 mA. Samples were scanned between 5° (2θ) and 60° (2θ) using a step size of 0.05° and a count time of 1 s using the Bragg–Brentano geometry. The morphology of the DAMN polymeric particles was assessed using a Thermo Scientific Apreo C-LV field emission scanning electron microscope (FE-SEM). The samples were dispersed by sonication in EtOH, deposited on glass slides, dried at 60 °C overnight in an oven and then coated with 4 nm chromium by sputtering using a Leica EM ACE 600. The images were obtained at 10 kV. Density data were acquired in an AccuPyc 1330 helium pycnometer from Micromeritics. The Brunauer–Emmett–Teller (BET) surface area and porous texture were evaluated by nitrogen adsorption-desorption isotherms obtained at -

196 °C using Micromeritics ASAP 2010 equipment. Before each measurement, the samples were degassed at 200 °C for at least 3 h.

*2.3. Catalytic activity test*

A commercial ammonium perchlorate ($NH_4ClO_4$, AP) oxidizer with an average particle size of 6 μm was received from SNPE, and it was used to evaluate the catalytic activity of the prepared DAMN polymers. They were thoroughly mixed with AP by a conventional physical mixing method in an agate mortar for 20 min and then studied by DSC-7 of Perkin Elmer as mentioned above. Five milligrams of AP samples and the corresponding mixtures were placed in aluminium pans closed with a pierced lid and dynamically heated from 30 to 500 °C at 10 °C/min and under a 20 ml/min dry nitrogen atmosphere. Each test was repeated several times to ensure consistent results.

## 3. Results And Discussion

*3.1. Bulk Polymerizations*

As indicated in the introduction, previous studies have described the behaviour of DAMN under dynamic thermal conditions [10,11,14]. **Fig. 1** shows an example of nonisothermal DSC experiments at a low β value of 2 °C/min. This DSC curve, under an inert nitrogen flow, clearly shows that the DAMN polymerization reaction occurs in the solid-state before the onset of the melting process and after this transition. However, these three well-defined processes cannot be independently viewed when the reaction is performed in the presence of air; in this case, the melting process is not observed, and the high exothermic peak corresponding to the MP appears sharper and slightly displaced at lower temperatures. From these DSC measurements, it was confirmed that the air hardly affects the DAMN SSPs, but they cause a higher exothermicity and a shift at a lower temperature of the MP [14]. These data provide guidance to analyse isothermal polymerization at the preparative scale in the presence of air. Thus, two isothermal experiments at 160 and 170 °C were planned to describe the DAMN polymerization in the solid-state, and temperatures of 190 and 200 °C were chosen to evaluate the MPs.

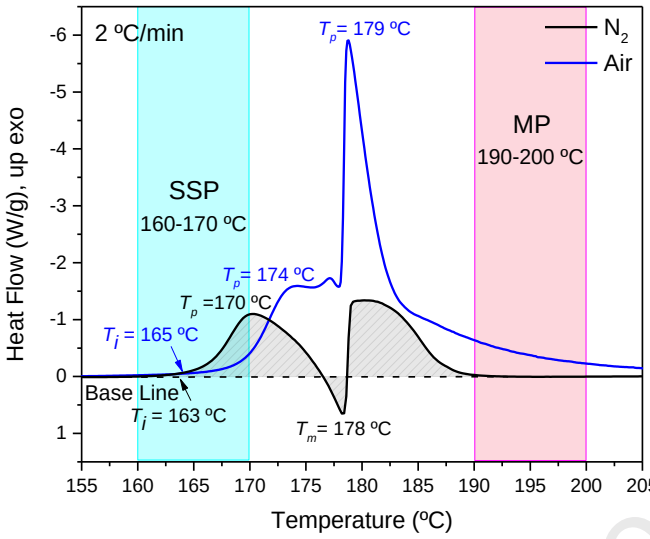


**Fig. 1**. DSC curves of the DAMN polymerizations for a β of 2 °C/min under different atmospheres.

It is important to note that DSC is a fairly appropriate technique to monitor these induced thermal polymerization reactions, but it truly is an indirect methodology, where a physical property can be related to the extension of the reaction, and therefore, the application of a gravimetric method at a preparative scale is essential to determine the final conversion achieved. Two series of experiments were carried out as described in the Materials and Methods section. In series 1, two phases were clearly observed in the vials after the corresponding reaction times (**Fig. 2**). The solid phases collected at the bottom of the vials were black powered solid with FTIR spectra with a very high resemblance to those obtained for DAMN polymerization under $N_2$ conditions [12], exhibiting broad and featureless bands in most of the spectral regions, suggesting a complex structure, as discussed in the next section (**Fig. 2b**). This result is in agreement with those previously reported by Mamajanov and Herzfeld, who proposed the formation of a polyaminoimidazole, such as the one indicated in the lower right part of this Figure [15].

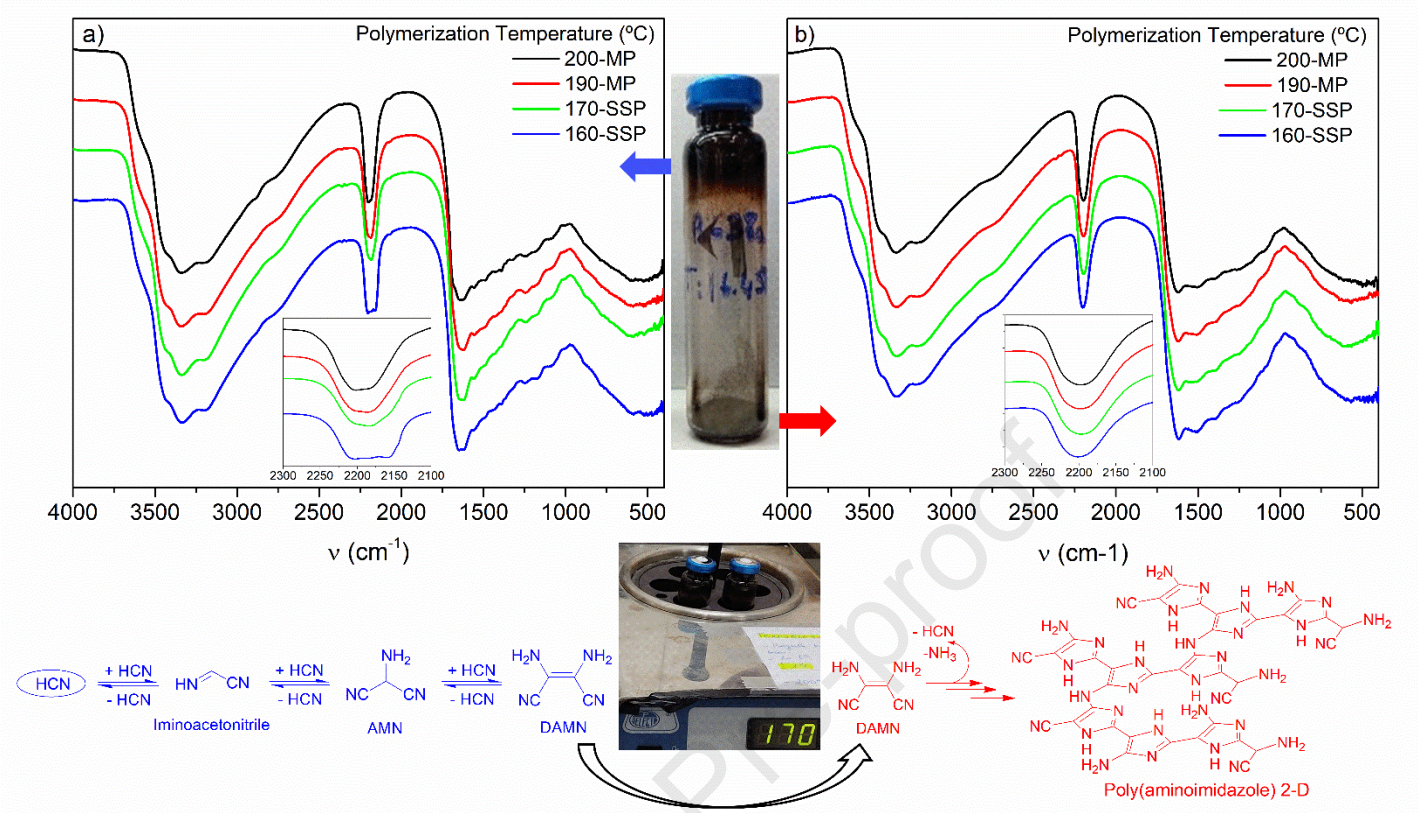


**Fig. 2**. FTIR spectra of the reaction products from the bulk thermal DAMN polymerizations using 20 ml vials sealed with Teflon set-ups (series 1), where a representative crude reaction sample is shown. **(a)** Upper part of the vials HCN polymers, as described in the text, and **(b)** bottom part of the vials DAMN polymers, based on the model proposed by Mamajanov and Herzfeld [15].

In contrast, in the upper parts of the vials, thick dark brown coatings were produced. These coatings can correspond to the liquid polymerization of HCN in the presence of $NH_3$ in the coldest upper area of the vials, given that the simultaneous release of HCN and $NH_3$ during DAMN polymerization was proven by TG *in situ* mass spectrometry (MS) [10-12]; herein, these processes could be directly observed together with the condensation of HCN and its lately polymerization (see **video** in the Supplementary Information). The IR spectra of these HCN polymers are shown in **Fig. 2a** and are quite similar to those of the DAMN polymers. Comparatively, only the band related to the nitrile groups, centred at ~2200 $cm^{-1}$, shows light differences, as is observed in the inserted plots in both figures. In fact, the evolution of this peak with the polymerization temperature for HCN polymers is very similar to that observed for the aqueous cyanide polymerizations with the reaction time, being

directly related to its profile with the conversion degree [20]. In this case, the first steps of the oligomerization of this weak acid until DAMN formation are indicated at the bottom left of the Figure 2.

To produce pure DAMN polymers, new experiments according to series 2 were performed, as described in the Materials and Methods section. Thus, once a simple, effective and reproducible synthetic methodology was developed, the yields of the DAMN bulk polymerizations were calculated (**Table 1**). Note that these polymer conversions decrease with the temperature increase, from 93% for an SSP at 160 °C to 85% when the polymerization temperature is 200 °C according to a MP. This fact might be related to the higher temperatures favouring a greater delivery of HCN and $NH_3$, increasing the secondary polymerization of HCN against DAMN polymerization, and therefore, the yields in pure DAMN polymers are lower. Significantly, no substantial differences were found between the results from series 2 and those previously reported for DAMN polymerizations under an inert atmosphere of $N_2$ [12]. Significantly, these yields are considerably higher than those found when pyrolytic g-$C_3N_4$ are prepared [4-6].

**Table 1.** Reactions parameters for DAMN polymerizations in air, yields, elemental analysis with atomic percentages in weight (wt), and C/N and C/H molar ratios of the resulting products. For comparative purposes, the polymerization times chosen for the polymerizations at 170 and 190 °C were the same as those used for the analogous polymerizations carried out under a $N_2$ atmosphere [12]. For 160 and 200 °C, the reaction times applied are based on the DSC results [10,11,14].

| Sample | Polymerization | | | Elemental composition | | | Molar ratio | |
|---|---|---|---|---|---|---|---|---|
| | T (°C) | Time (min) | Yield (%) | C (wt %) | H (wt %) | N (wt %) | C/N | C/H |
| 160-SSP-Air | 160 | 270 | 92.9 ± 0.6 | 42.9 ± 0.2 | 3.4 ± 0.1 | 45.9 ± 0.5 | 1.09 | 1.05 |
| 170-SSP-Air | 170 | 180 | 88.6 ± 0.6 | 43.0 ± 0.2 | 3.3 ± 0.1 | 45.5 ± 0.5 | 1.10 | 1.09 |
| 190-MP-Air | 190 | 20 | 85.3 ± 0.7 | 43.3 ± 0.3 | 3.2 ± 0.1 | 45.0 ± 0.5 | 1.12 | 1.13 |
| 200-MP-Air | 200 | 10 | 84.7 ± 0.4 | 43.5 ± 0.3 | 3.3 ± 0.1 | 45.2 ± 0.5 | 1.12 | 1.10 |

*3.2. Structural, physical and morphological properties of DAMN polymers*

The samples were examined by elemental analysis to establish the atomic percentages, which are practically independent of the reaction temperature, and whether the polymerization is carried out in the solid-state or in melt (Table 1). In addition, the atomic

C/N and C/H ratios (Table 1) give more direct detail on the relative abundances of the elements and therefore also clues to which molecules have been eliminated than mass percentages. For example, just eliminating $NH_3$ would create a C/H > C/N. In contrast, if elimination of HCN dominates, this would keep the ratios close to 1. The reported experimental C/N and C/H ratios are very similar and slightly greater than one, which implies that N and H are eliminated in small amounts relative to C. These results can be compared with those obtained for samples synthesized under a nitrogen atmosphere; thus, in this case, values close to 1.10 were found [12].

On the other hand, the practical absence of oxygen content in all the samples analysed, both those obtained in air and under an inert atmosphere or polymerized in solid-state or melt, is consistent with the fact that oxygen is not incorporated during bulk thermal DAMN polymerizations in the presence of air. The presence of oxygen could affect the cross-linking and facilitate the cyclization and dehydrogenation reactions, the latter according to elemental analysis. These side processes could be associated with a density change of these materials, as has been described during the thermal stabilization process of other related polymers [21]. However, the densities of our DAMN polymers were quite similar (**Table 2**) except for a slight increase as the temperature of the polymerization process decreased. At this point, it is important to note that according to these data, the DAMN-derived polymeric materials have a great similarity with recently described amorphous g-$C_3N_4$ materials, which are obtained from the pyrolysis of formamidinium halide salts, observing a loss of $NH_3$ and HCN and presenting a mass fraction of 40-50% nitrogen content [8].

It seems that the presence of air during DAMN thermal polymerization does not modify the macromolecular structure of the final products. To confirm this result, a more exhaustive study using several spectroscopic and analytical techniques was developed. Thus, FTIR parameters are very valuable to verify the extension of the reactions (EOR), and at the same time, they allow us to extract information about the microstructure of the DAMN polymer generated. Normalized absorbance IR spectra of the samples obtained are displayed in **Fig. 3a**. To facilitate comparison of the spectra, different semiquantitave ratios have been calculated, as is common when analysing this type of polymeric material [22], and similar indices have also been applied in the study of g-$C_3N_4$ [23]. The values of the EOR were calculated from the FTIR spectra taking the relative intensity of the band at ~1625 $cm^{-1}$ [C=C and/or $(C=N)_n$] and that of the nitrile groups at ~2195 $cm^{-1}$ (Table 2).

Comparatively, no significant differences were found between the DAMN polymers described in this document or with the samples obtained under $N_2$ [12], in good agreement with the above results obtained by means of elemental analyses.

**Table 2.** Physical and morphological properties of the resulting products.

| Sample | Density ($g/cm^3$) | EOR by FTIR (%) | BET surface area ($m^2/g^1$) | |
|---|---|---|---|---|
| | | | High pressure | Low pressure |
| 160-SSP-Air | 1.65 | 57.8 ± 0.2 | 1.20 | 1.20 |
| 170-SSP-Air | 1.63 | 59.4 ± 1.2 | 2.86 | 2.66 |
| 190-MP-Air | 1.62 | 59.9 ± 1.0 | 3.41 | 3.30 |
| 200-MP-Air | 1.61 | 58.4 ± 1.2 | 3.37 | 3.30 |

These spectra are similar to those of g-$C_3N_4$ from formamidinium halide salts (with a greater contribution of $–NH_x$ and -C≡N groups in our samples, see Figure 3 in reference [8]). Nonetheless, they present significant differences with respect to those conventional g-$C_3N_4$ obtained from usual precursors (for example, see Figure 7 in reference [23]) since herein, the characteristic band at approximately 800 $cm^{-1}$, associated with triazines and that confirms the presence of these rings, is absent (inserted plot). Moreover, although it is possible to postulate the formation of triazine-based macrostructures such as those from DAMN, as discussed in the last section, these spectroscopic data (and following) reveal clear structural differences between the DAMN-derived polymers and traditional g-$C_3N_4$ materials.

Only subtle differences between our samples were found when spectral subtractions were carried out (**Fig. 3b**). Thus, the subtraction between the spectrum of the sample160-SSP with respect to that of 200-MP shows a slight decrease in absorption in the N-H stretching region between 3700 and 3300 $cm^{-1}$; therefore, a smaller number of amine groups should be present in the polymer samples obtained in the solid-state. In addition, the negative peaks at ~2170 $cm^{-1}$ confirm the presence of a β-enamino nitrile and/or β-imino nitrile corresponding to a nitrile moiety in conjugation with a double bond [24]. Finally, positive bands are found in the broad region between 1730 and 930 $cm^{-1}$, where the typical stretching modes of C-N heterocycles, such as diazine rings, appear [25], with relevant peaks at 1612, 1509 and 1390 $cm^{-1}$ (inserted plot), where a deconvolution method has been applied. From this last result, we think that more cyclization reactions, probably between amino and cyano

groups, as indicated in Fig. 3b, could take place when the polymerization reaction is performed in the solid-state.

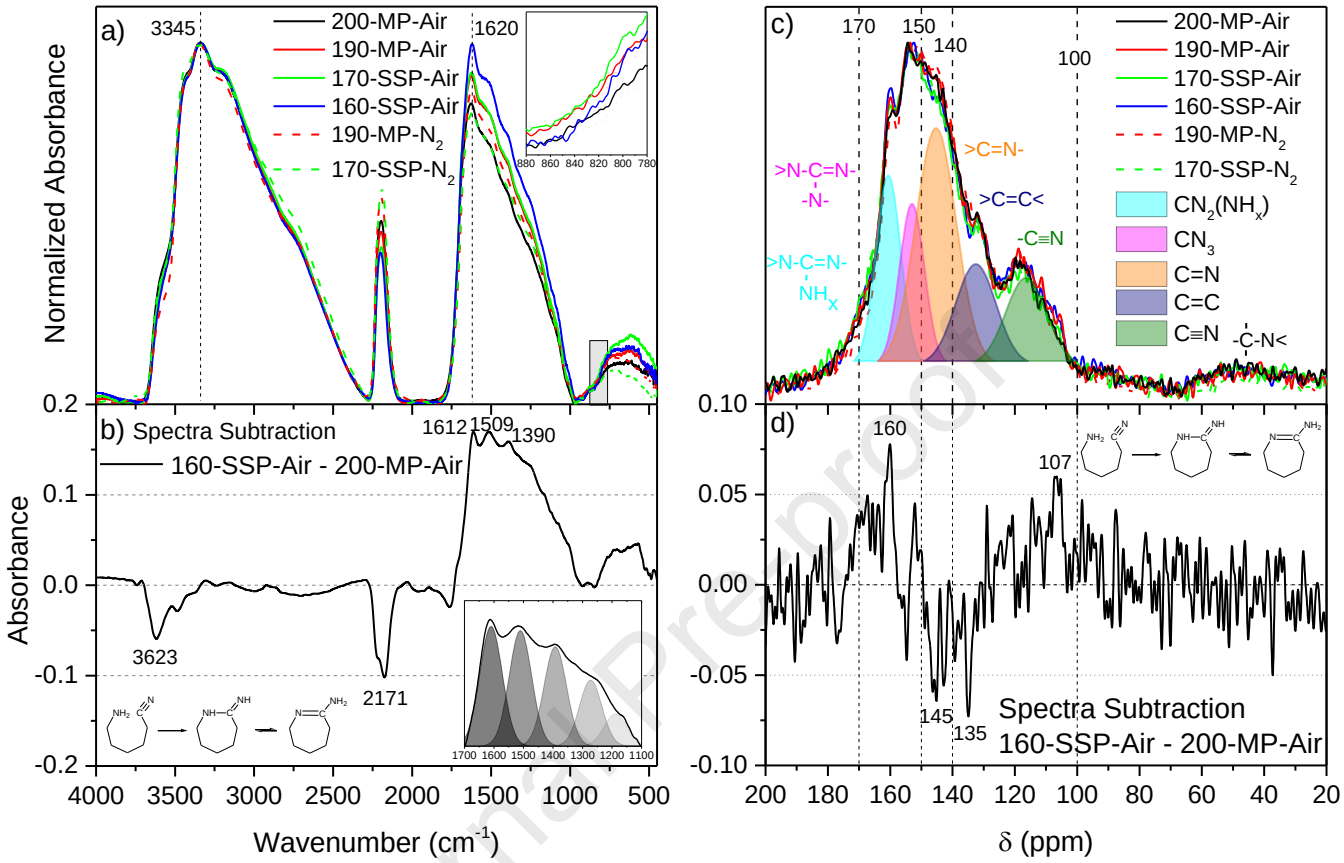


**Fig. 3. (a)** Normalized FTIR spectra with baseline correction of the DAMN polymers synthesized by SSP and MP (series 2); **(b)** subtractions of the FTIR spectra; **(c)** solid-state $^{13}C$ NMR spectra of DAMN polymers synthesized by SSP and MP; **(d)** subtraction of the NMR spectra.

Similar conclusions were drawn when the samples under study were analysed by solid-state NMR spectroscopy. Thus, the $^{13}C$ CP-MAS spectra of the products obtained in the presence of air and those registered from the samples prepared under a nitrogen atmosphere are remarkably similar (**Fig. 3c**). This same assertion can be extrapolated when these spectra are compared with NMR signals of g-$C_3N_4$ obtained from the formamidinium cation (see Figure 11 in reference [8]). These broad and asymmetric resonances are diagnostic of heterogeneous and amorphous materials, and obtaining information on the nature of corresponding building blocks is complicated. However, the spectra of classical g-$C_3N_4$ show two main signal groups in a 2:1 ratio, and the signal ranging from 170-160 ppm

is assigned to amine-bearing carbons, $CN_2(NH_x)$, while the other signal ranging from 160 to 150 ppm is due to the $sp^2$ species linked trigonally to three atoms within the triazine or heptazine rings and not directly connected to any N-H functional groups, $CN_3$ [6]. The line shapes of our spectra in this region may suggest relative populations of the $CN_2(NH_x)$ and $CN_3$ moieties, properly of both s-triazine and/or tri-s-triazine polymers, in the DAMN polymers; however, it is important to note that in the IR spectra, no signals associated with the out-of-plane bending vibrations of these heterocyclic systems were detected.

Resonances close to 150 ppm can be assigned to carbons bound to two nitrogens, and the breadth of this imine region (C-C(R)=N-) may be due to the heterogeneity in R; finally, the signals at 135–100 ppm can be assigned to carbons in the carbon–carbon double bond (C=C) or the carbon-nitrogen triple bond (C≡N) functionality. In addition, the broad unresolved resonance at 60–100 ppm can be related to the presence of $sp^3$ carbons (C-N) [26,27]. The deconvolution of five relevant resonances of these spectra could help to better interpret this complex and heterogeneous system. Thus, the strong featureless resonances at 180–135 ppm are from carbons in the carbon-nitrogen double bond functionality (C=N), and the contributions of the three corresponding Gaussian peaks shown in this figure are 18, 15 and 37% for the consecutive peaks centred at 161, 153 and 145 ppm, respectively. Therefore, approximately 70% of the different imine groups or C atoms of heterocyclic containing N must be the major component of this polymeric system. The percentages of $Csp^2$-$Csp^2$ and nitrile groups are 16 and 14%, respectively; this last contribution is relatively low considering the semiquantitative parameter obtained from the FTIR analyses.

To find other structural differences beyond those obtained from the deconvolution methodology, in a recurring way, spectral subtractions of NMR data were carried out, as displayed in **Fig. 3d**. Only insignificant differences were found between the spectra of the samples obtained at 160 °C and the sample prepared at 200 °C; thus, positive peaks with intensities higher than 5% are observed at low-field, approximately 160 ppm, suggesting that $CN_2(NH_x)$ fragments and in the nitrile zone at ~105 ppm must be present to a greater extent in the sample prepared at 160 °C. On the other hand, several negative peaks are found at 145 and 135 ppm, which could be part of the carbon skeleton of the different segments or blocks, discussed later in the section 3.2.

Derivative thermogravimetry (DTG) curves have been used previously as thermal fingerprints for HCN-derived polymers when spectroscopic data are not capable of

distinguishing samples synthesized under different conditions [28-30], such as the present case. **Fig. 4a** shows the DTG and TG profiles for the DAMN polymers under study. There were no significant differences between the distinct samples regardless of the synthetic conditions used. Thus, the temperatures of the maximum degradation rate are ~ 675 °C for all samples, although the sample prepared at 190 °C from $N_2$ presents the highest value of 690 °C, while the sample prepared according to SSP at 170 °C under air exhibited the lowest value, with a temperature of 667 °C, as indicated in this figure. This fact may be related to its crystallographic properties, which are described as follows.

In **Fig. 4b,** the normalized XRD patterns and the corresponding data collected in **Table 3** reveal the low impact of the temperature and the atmosphere on the internal order and arrangement of the DAMN polymers. All the polymeric macrostructures exhibit a broad diffraction centred at ~ 27°, which is usually assigned as the "002" feature of a graphitic structure, indicating the interlayer spacing dimension. A second broad feature with lower intensity is also observed in the 10-16° 2θ range, which in the case of graphitic $C_xN_yH_z$ materials prepared by thermal condensation from molecular precursors has been associated with structural correlation occurring between heptazine ring units and the presumed "graphitic" layer [6,31]. However, this secondary peak is not observed in those samples obtained from formamidinium halide salts as precursors, indicating amorphous, disordered in-plane and out-plane materials [8]. In addition, it must be mentioned that other diffraction peaks were not observed, which have been thoroughly studied in conventional g-$C_3N_4$ materials using discrete Fourier transform and direct experimental evidence [31].

Quantitative curve fitting was conducted for a deeper understanding of the XRD data, and some parameters were calculated via Bragg's law and the Debye-Scherrer equation (Table 3). Thus, careful analyses of these data demonstrated that the full width at half maximum (FWHM) of the reflection from the (002) plane was broader for the lower polymerization temperature, sample 160-SSP-Air. This indicates a further reduction in the nanoscopic crystallite size according to the Scherrer equation. In addition, the two samples obtained under an inert atmosphere present a higher crystallinity overall than that prepared at 190 °C from the molten state.

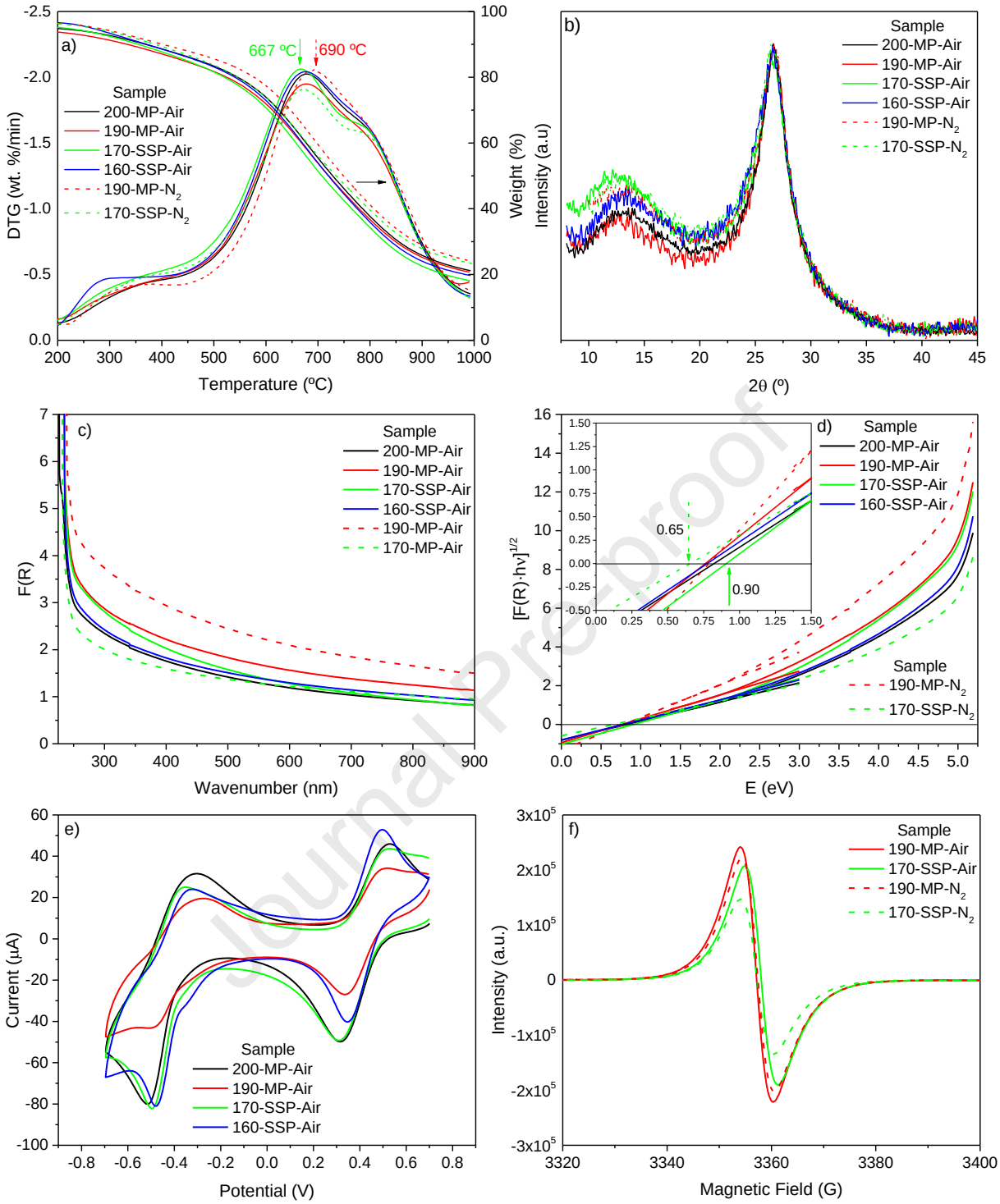


**Fig. 4. (a)** DTG and TG curves, β = 10 °C/min under an argon atmosphere, **(b)** powder XRD patterns, **(c)** UV–Vis diffuse reflectance spectra, **(d)** Tauc plot (indirect allowed band gap setting) of the Kubelka-Munk transformation of the diffuse reflectance data, **(e)** cyclic voltammograms of electrodes modified with the four DAMN polymers, measured in 0.1 M $NaClO_4$ at a scan rate of 100 mV/s, and **(f)** EPR spectra recorded at room temperature of DAMN polymers synthesized by SSP and MP.

**Table 3.** XRD properties and fitting parameters for the main peak of the DAMN polymers obtained both in air and $N_2$ atmosphere. [a] 170-SSP-Air sample peak area normalized to 100 units.

| Sample | First peak (°) | *d* (Å) | Peak maximum (002) (°) | $d_{002}$ (Å) | Peak area[a] (au) | FWHM (°) | Scherrer crystallite size (nm) | Crystallinity (%) |
|---|---|---|---|---|---|---|---|---|
| 160-SSP-Air | 13.02 | 6.79 | 26.48 | 3.36 | 109 | 3.70 | 2.3 | 47 |
| 170-SSP-Air | 12.28 | 7.20 | 26.53 | 3.36 | 100 | 3.26 | 2.6 | 52 |
| 190-MP-Air | 13.59 | 6.51 | 26.63 | 3.34 | 108 | 3.12 | 2.7 | 53 |
| 200-MP-Air | 13.29 | 6.66 | 26.60 | 3.35 | 113 | 3.15 | 2.6 | 50 |
| 170-MP-$N_2$ | 13.14 | 6.73 | 26.44 | 3.37 | 110 | 3.36 | 2.5 | 56 |
| 190-MP-$N_2$ | 13.52 | 6.54 | 26.59 | 3.35 | 111 | 3.26 | 2.6 | 66 |

On the other hand, in contrast with the yellow or brown powders habitually exhibited for classical g-$C_3N_4$ materials, our black samples absorb all the visible wavelengths (**Fig. 4c)**, as also occurs in hydrogenated g-$C_3N_4$ [8]. The Tauc plot for the six polymeric samples was also represented to estimate their optical band gap (**Fig. 4d**). All of them present a value of indirect band gap between 0.65 and 0.9 eV (inserted plot). It is important to mention that these values are higher than those estimated for the g-$C_3N_4$ materials obtained from fomamidinium halide salts [8], but they are lower than more conventional yellowish g-$C_3N_4$ samples that present a band gap energy range of approximately 2.3 eV [1-3].

Electrochemistry is another method to determine the band gap. **Fig. 4e** shows the cyclic voltammograms (CVs) of electrodes modified with the four polymers in 0.1 M aqueous $NaClO_4$. All materials show similar CVs, with two quasireversible electrochemical systems at near potentials, indicating the same electroactive functional groups. Nevertheless, these potentials differ from those observed with the 170-SSP-$N_2$ and 190-MP-$N_2$ compounds and shift towards more positive potentials [12]. These differences can indicate different environments for the functional groups that hinder oxidation processes and facilitate reduction processes. It is known that the formal potentials of the systems **(Fig. 4e)**, calculated as the average of $E_{pc}$ and $E_{pa}$, can be related to the p- and n-doping status of a semiconductor material and used to calculate the HOMO (highest occupied molecular orbital), the LUMO (lowest unoccupied molecular orbital), and the HOMO-LUMO band gap ($E_g$) [32,33]. As usual, for these calculations, the absolute potential for the standard hydrogen electrode (SHE) and the potential difference

between the SCE and SHE of 4.43 eV and 0.24 V, respectively, were used. **Table 4** shows the results obtained with the polymers prepared in the presence of air and the values obtained with the 170-SSP-$N_{2-}$ and 190-MP-$N_2$-modified electrodes [12], measured from the CVs at a scan rate of 100 mV/s. These data demonstrate that the air-synthesized polymers show a greater band gap than the nitrogen-synthesized polymers, while there are no significant differences between the polymers obtained in the presence of air at different temperatures. In addition, they present a correct correlation with those obtained from the Tauc plot mentioned above. These results open up the possibilities of future studies about the usefulness of these organic semiconductors, whose potential applications in several fields, such as biomaterials [34], protective coatings [35,36], capacitors [9], filtration devices [37], photocatalysts [38], and biosensors, have already been well documented [12].

**Table 4.** Electrochemical data obtained from the peak potential values.

| Sample | $E^0_{pa}$ (V) | $E^0_{pc}$ (V) | HOMO (eV) | LUMO (eV) | $E_g$ (eV) |
|---|---|---|---|---|---|
| 160-SSP-Air | 0.42 | -0.41 | 5.16 | 4.33 | 0.83 |
| 170-SSP-Air | 0.41 | -0.43 | 5.15 | 4.31 | 0.84 |
| 190-MP-Air | 0.42 | -0.39 | 5.16 | 4.35 | 0.81 |
| 200-MP-Air | 0.42 | -0.42 | 5.16 | 4.32 | 0.84 |
| 170-SSP-$N_2$ | -0.06 | -0.62 | 4.68 | 4.12 | 0.56 |
| 190-MP-$N_2$ | -0.06 | -0.62 | 4.68 | 4.12 | 0.56 |

EPR spectra of some polymers considered herein show that they present a substantial quantity of long-lived organic free radicals, according to a single unresolved symmetric signal centred at g = 2.008, which seems to indicate radicals containing only one unpaired electron (S = ½) (**Fig. 4f**). Qualitatively, the signal intensity increases with the polymerization temperature and with the presence of air in the reaction environment. These results are in agreement with the paramagnetic nature of other HCN-derived polymers previously reported [39,40] and layered g-$C_3N_4$ materials, such as those obtained from biomolecules [7].

Knowledge of additional information about the morphological and textural properties of our C=N systems is of interest considering that these properties could be conveniently modulated for further applications [13] and to understand the differences produced by the SSP and MP processes. Thus, morphological investigation of the prepared samples was performed by SEM (**Fig. 5**). In general, both DAMN polymers prepared under an air atmosphere present no well-defined particle shapes, and as can be observed, the differences produced by the SSP and MP processes are irrelevant from the analysis of these images. In addition, the BET surface area of the four samples was measured by $N_2$ adsorption–desorption isotherms, finding lower values for the DAMN polymer prepared at the lowest temperature (Table 2).

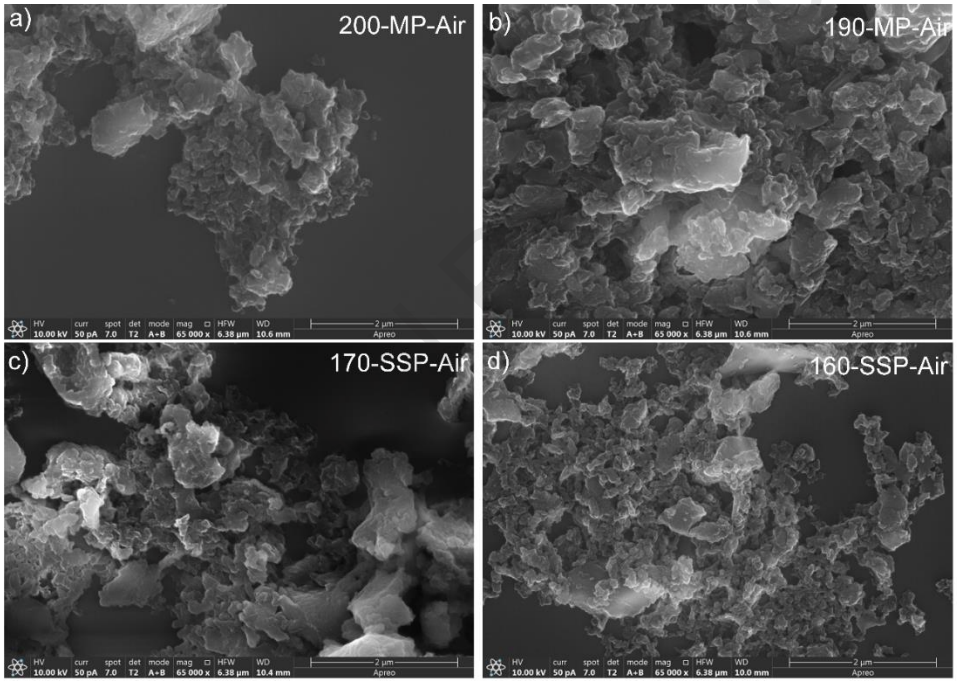


**Fig. 5.** SEM images of representative samples of DAMN polymers synthesized by MP (**(a)** and **(b)**) SSP (**(c)** and **(d)**) and under air atmosphere.

*3.2. Applications of DAMN polymers in catalysts*

Combustion catalysts have a wide range of applications in the field of aerospace propulsion and, more concretely, in composite propellants based on AP, as previously mentioned. The catalysts most commonly applied are transition metal oxides, ferrocene and its derivatives, metal-organic frameworks and carbon materials (such as carbon nanotubes and graphene). Among 2-D materials, emerging transition metal carbides and

nitriles, known as MXenes [41], g-$C_3N_4$ and their composites, have also been explored, as they have been systematically reviewed [42] and discovered in this catalytic field by Peng and coworkers [43]. Motivated by the use of these C-N metal-free catalysts in this singular application, we decided to explore our materials under study; thus, their catalytic performances on the thermal decomposition of AP were studied by DSC measurements.

**Fig. 6a** displays the DSC curves of pure AP and 10% AP in wt of the DAMN polymers for a β of 10 °C/min in the range of 50-500 °C and using open pans under a flow of nitrogen. These experimental conditions and proportions were selected based on the study of Li et al. [43]. The known thermal decomposition of pure AP under these conditions presents two exothermic peaks: the first peak takes place in the low-temperature decomposition stage at approximately 310 °C, with a low intensity that looks very faint; and the second peak, in the high-temperature decomposition regime, appears as an asymmetric and intense peak from 345 to 465 °C. In addition, the endothermic peak at ~245 °C is assigned to the crystallographic transition of AP from orthorhombic to cubic, according to the extensive literature on the properties of AP in general, particularly its thermal decomposition [44]. The addition of the different catalysts resulted in significant changes; thus, these free-metal organic additives based on DAMN polymers shift the AP thermal decomposition process to lower temperatures and considerably reduce its temperature range. The 170-SSP-Air sample exhibits an unusual DSC gram profile, with a sharp exothermic peak at 415 °C. A similar catalytic effectiveness is clearly observed for both samples prepared through an MP, exhibiting a comparable behaviour; however, in this case, two well-defined peaks are now observed, with the one that appears at the higher temperature being the one with the highest exothermicity. However, the AP thermal decomposition in the presence of the 160-SSP-air catalyst presents a different calorimetric trace compared to the other samples, where the most intense peak is now located first at the lowest temperature, in this case at 384 °C. On the other hand, in **Fig. 6b**, two catalysts prepared in the presence of air at 170 and 190 °C are now compared with those samples produced under an inert atmosphere. From these DSC-grams, it can be concluded that these last catalysts develop a better catalytic activity during the AP thermal decomposition and, above all, that samples were obtained according to an MP procedure.

In an attempt to analyse the essential structure-property relationship, **Fig. 6c** and **6d** show a parameter related to the catalytic effectiveness of the DAMN polymers in the

AP thermal decomposition in front of different textural, crystallographic, and electronic properties. This parameter $\Delta T$ was estimated from the decrease in the maximum exothermic peak temperature illustrated in Figures 6a and 6b. Thus, for the 160-SSP-Air sample, $\Delta T = T_{p\text{-}AP}$ (pristine AP sample) – $T_{p\text{-}DAMN\ Polymer}$ = 465-384 = 81 °C is found; in principle, a higher catalytic activity, although it exhibits the lowest value of surface area, presents a lower crystallinity value, and at the same time a reduction in the nanoscopic crystalline size, as is clearly seen in Fig. 6c. It is surprising that when this parameter reflecting the catalytic effectiveness is compared with those samples prepared in an inert atmosphere, the best results are found for the 190-MP-$N_2$, Fig. 6d. Thus, this sample, with the highest $\Delta T$ = 85 °C, also shows a low BET value, but on the contrary, it reveals the highest crystallinity and jointly the lowest band gap values estimated by electrochemical measurements. Furthermore, in this figure, it is possible to see how $\Delta T$ increases in the same way that crystallinity does as we move from left to right.

These apparently contradictory results are not trivial, and it must be taken into account that the thermal decomposition of AP still remains largely unrevealed [44]. However, from the data of Li et al., it is possible to calculate a value of $\Delta T$ = 70 °C for their g-$C_3N_4$ catalysts (Figure 2b in reference [43]). Additionally, DAMN polymers present promising potential for the development of energetic coordination polymers, which have good application prospects as combustion promoters of solid propellants [45]. In this way, a recent work is described with a greater and deeper extent this singular application [46] and in new fields, such as photocatalysis, where poly-HCN nanofibers have demonstrated high potential [38].

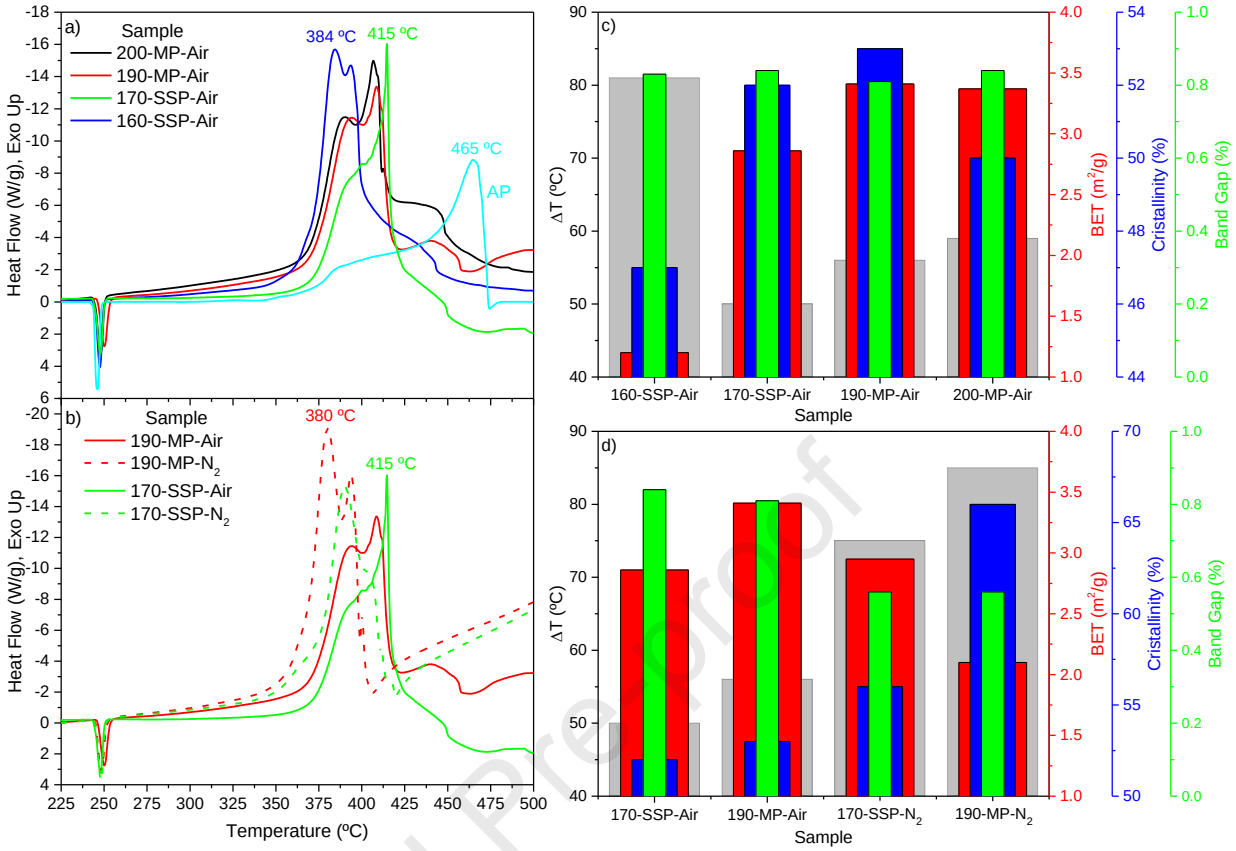


**Fig. 6**. **(a)** DSC curves of pure AP and its mixture with the catalysts based on DAMN polymers prepared at 10 wt% and a β of 10 °C/min, **(b)** DSC curves of the mixture AP plus different catalysts at 10 wt%, air *versus* $N_2$, for a β of 10 °C/min, **(c)** and **(d)** comparison between catalytic activity, estimated by decreasing the decomposition temperature, and different physical parameters for the DAMN polymers.

### *3.3. Mechanistic considerations*

Taking into account the spectroscopic results, air seems to have no effect on the formation of DAMN-derived polymeric macrostructures. Only variations in the values of the band gap energy, the redox potentials and certain crystallographic parameters were observed. These differences may be due to work in the presence of air that leads to several structural defects, disorder at the grain boundaries, and three-dimensional quantum size effects. This fact could have the following justification, it is well known that amino groups are very sensitive to oxygen (oxidation), especially at elevated temperatures. The oxidation rate of the amino groups is expected to be much faster than the polymerization rate. The starting oxidation temperature should be also significantly lower than the

starting polymerization temperature. However, no distinction was taken into consideration between air and an inert atmosphere in the following mechanistic proposals. Moreover, under air or nitrogen atmospheres, the gases evolved during the polymerizations were the same, mainly HCN and $NH_3$ in apparent equimolar quantities, in accordance with previous studies [10-12] and the data collected here. Therefore, dehydrocyanation and deamination are considered the principal elimination reactions involved during the DAMN polymerization processes.

In **Scheme 1**, a hypothetical mechanism based on the tautomeric balance enamine-imine and considering three DAMN molecules, trimerization, is shown in the first step. This thermally activated initiation stage will be controlled by dynamic imine chemistry, and it is important to take into account the inherent 'proof-reading' and 'error checking' associated with its reversible reactions. In this case, the formation of a poly*gem*-diamine takes place through a transimination reaction, which can decompose either via deamination (Route 1) or with HCN elimination (Route 2), or even with the loss of $NH_2$-CN, or simultaneously HCN plus $NH_3$; these last two not contemplated in this scheme for simplicity. Aspects of Routes 1 and 2a were discussed elsewhere [10,12], and it is only necessary to introduce several clarifications. On the one hand, the polyaminoimidazole, the same as that shown in Figure 2, could undergo additional intramolecular cyclization reactions to reach a new polymeric architecture with fused rings. On the other hand, in Route 2b, the formation of novel polycyclic heteroaromatic oligo-structures, concretely constituted by pyrazine and pyrimidine rings, following amine-nitrile intramolecular cycloadditions in a second stage is proposed. This trimer based on six-membered rings with two heteroatoms is capable of evolving intermolecularly, similar to how polyaminoimidazole does, to achieve different planar conjugated macrostructures, where rearrangement N–N bond formation reactions must be considered. Following the same mechanistic sequence, in Route 1, a symmetric trimer supporting two pyrazine rings is obtained, which can subsequently condense up to a 9-mer oligomer formulated in this scheme. These polymeric systems, particularly those based on linked pyrazine and pyrimidine rings, present a macromolecular architecture similar to that exhibited by g-$C_3N_4$. In addition, the corresponding chemical shift δ (ppm) of the carbon in the simulated $^{13}C$ NMR spectra, calculated from ChemDraw Professional 15.0 software, can be observed in this scheme. Some of these resonances fit with the experimental signals shown in Figure 3c previously discussed. It is also worth mentioning that the theoretically

calculated C/N and C/H values for the 9-mers obtained from Route 2 are close to the experimental data collected in Table 1.

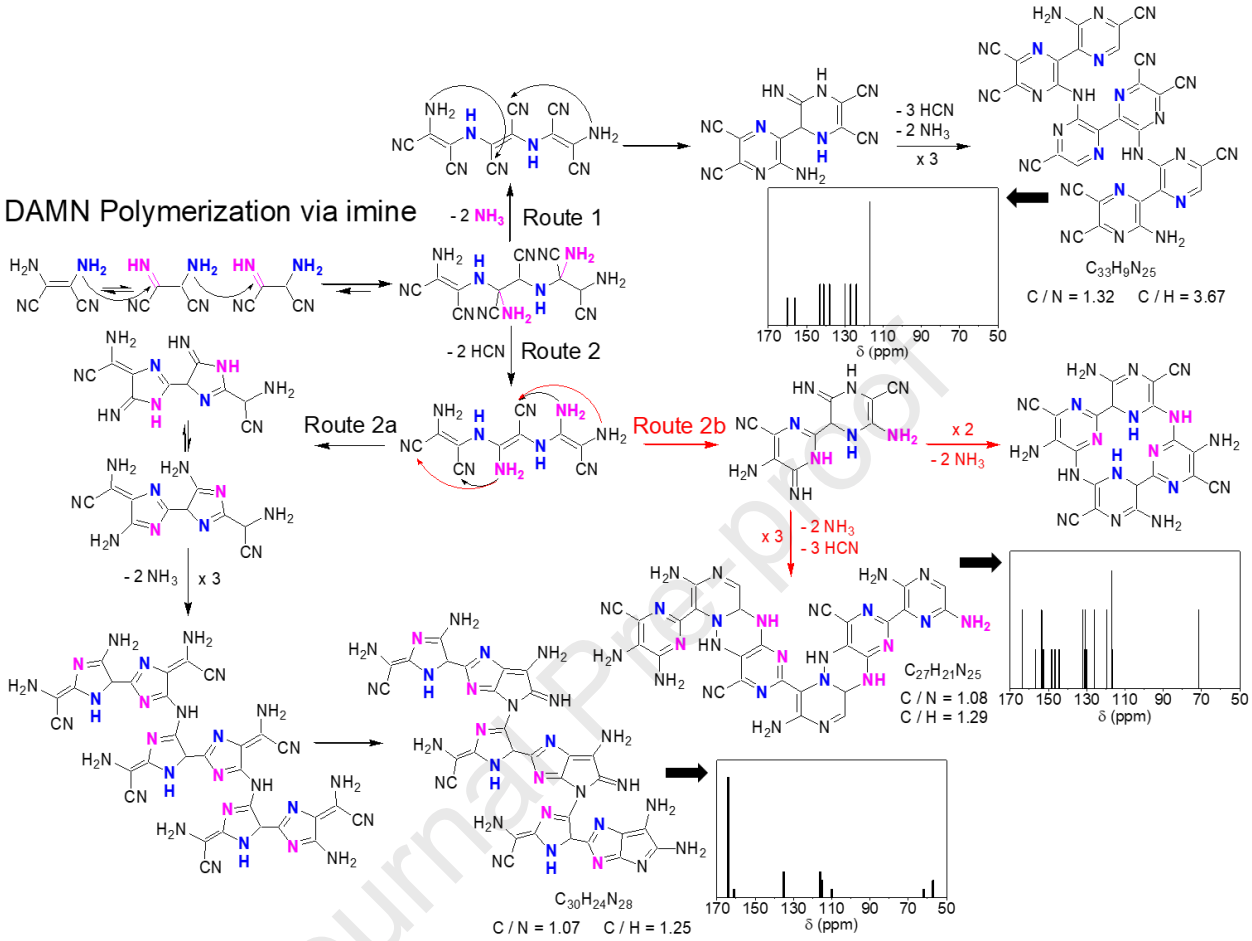


**Scheme 1**. Proposed synthetic routes with an initiation stage via imine for DAMN thermoself-polymerization.

However, it must be kept in mind that the tautomerization of DAMN in the solid-state can be questionable [47] and that cyano chemistry plays a fundamental role in the field of materials design, concretely being an important means for the construction of nitrile polymers, such as polyacrilonitrile widely used to produce carbon fibres and nanofibers, and cyano-based resins, such as phthalonitriles and related systems [21,48]. Thus, in **Scheme 2**, several rational synthetic routes are suggested based on the electrophilicity of the carbon centre of the nitrile group, although at the time, they were not critically analysed and discussed [9, 49]. They can lead to a variety of possible fully

conjugated ladder polymers consisting of continuously fused rings and/or extended structures from the continued elimination of $NH_3$, as this is also present during pyrolytic condensation to synthesize g-$C_3N_4$ materials.

Thus, as in Route 1 and for consistency, three DAMN molecules are also considered. During the step-growth polymerization, the initial formation of a linear 3-mer occurs by a polyaddition between amine and cyano groups, which can evolve to aminoimidazole units by means of intramolecular cyclization between neighbouring these same functional groups, Route 1a. This trimer based on imidazole rings, but in this case bridged with a =C-$NH_2$ group, can condense in distinct π-conjugated polymeric systems, in which the backbone units are mainly fused pentagonal heterocyclic rings, after a ladderization step with ammonia elimination. In a similar way to that presented in Scheme 1, a heterocyclic trimer based on six-membered rings can be obtained, Route 2b. This cyclic trimer can also undergo a ladderization process to yield different self-coupled products in the next stage, with the driving force of these last steps being the high conjugation of the formulated systems [50,51]. In Route 2, the initiation is by the amino group of DAMN, but after a first addition, a cascade reaction could take place through a nucleophilic attack on the carbon atom of an adjacent nitrile group and induce it to cyclize, leading to the formation of an oligomeric iminodiaminopyrrole. This trimer, via deamination and annulation reactions, can reach a fully conjugated ladder structure, which can condense in a subsequent stage by having imino and amino end functional groups.

An alternative cyclopolymerization not proposed to date for DAMN is illustrated in Route 3, forming a 1,3,5-triazine ring skeleton through the intermolecular condensation of three nitrile groups, probably being autocatalysed by amine groups of a DAMN molecule. This triazine, which is a key molecule in the synthetic route for g-$C_3N_4$, is capable of undergoing intramolecular cyclization to produce a trimer composed of four fused rings, which evolve through a condensation reaction to yield the layered oligomeric 6-mer system postulated here. This route is explained in terms of a mechanism based on the relative stability of the intermediate nitrilium salts that are formed through a reversible pathway [52], and it has been suggested in different nitrile polymers, such as in dicyanoimidazole resins based on DAMN [48].

At this point, and jointly examining the two mechanistic strategies postulated, the following considerations can be argued. First, it is necessary to indicate that all these

approaches to forming these C-N polymers consist of at least three stages, and this is in accordance with a multistep autocatalytic kinetic model described in a recent study [14]. On the one hand, polymerization via imine is deeply conditioned by thermally induced tautomerization of DAMN in the initiation step and pioneering works on the structure of DAMN given physical evidence that the HCN tetramer exists as DAMN, unlike its tautomeric form aminoiminosuccinonitrile, both in the crystalline state and in dilute solutions in neutral solvents at ordinary temperature [47]. However, both routes of Scheme 1 justify the loss of $NH_3$ and HCN during the course of the polymerization reactions, and in general, this mechanism is supported by the high reactivity of the primary imine group of the DAMN tautomer, which is in line with the robustness of the thermal polymerization reactions even in the solid state.

On the other hand, the synthetic pathways via nitrile of Scheme 2 do not contemplate HCN elimination, although a probable initial dehydrocyanation of DAMN to generate the HCN trimer, AMN, can also be considered [15], as illustrated in Figure 2, which would polymerize instantly due to its instability [53,54], possibly also with loss of HCN and $NH_3$ [55]. This could be a collateral process to the DAMN bulk thermal polymerization, but yielding as well black solids with very similar vibrational spectroscopic data to those discussed herein [55]. Finally, it is important to point out that some of the macrostructures proposed in Scheme 2 do not adequately match the spectroscopic and compositional data obtained experimentally. This fact may lead one to think that the most likely configuration of these DAMN polymers must be a rather complex macrostructure with different segments or blocks formed by dinitrogen heterocycles, such as imidazole and pyrazole rings, and noncyclic subunits, supporting mainly imine but also enamine groups [12], in line with the conclusions achieved by Ciria-Ramos et al. [8].

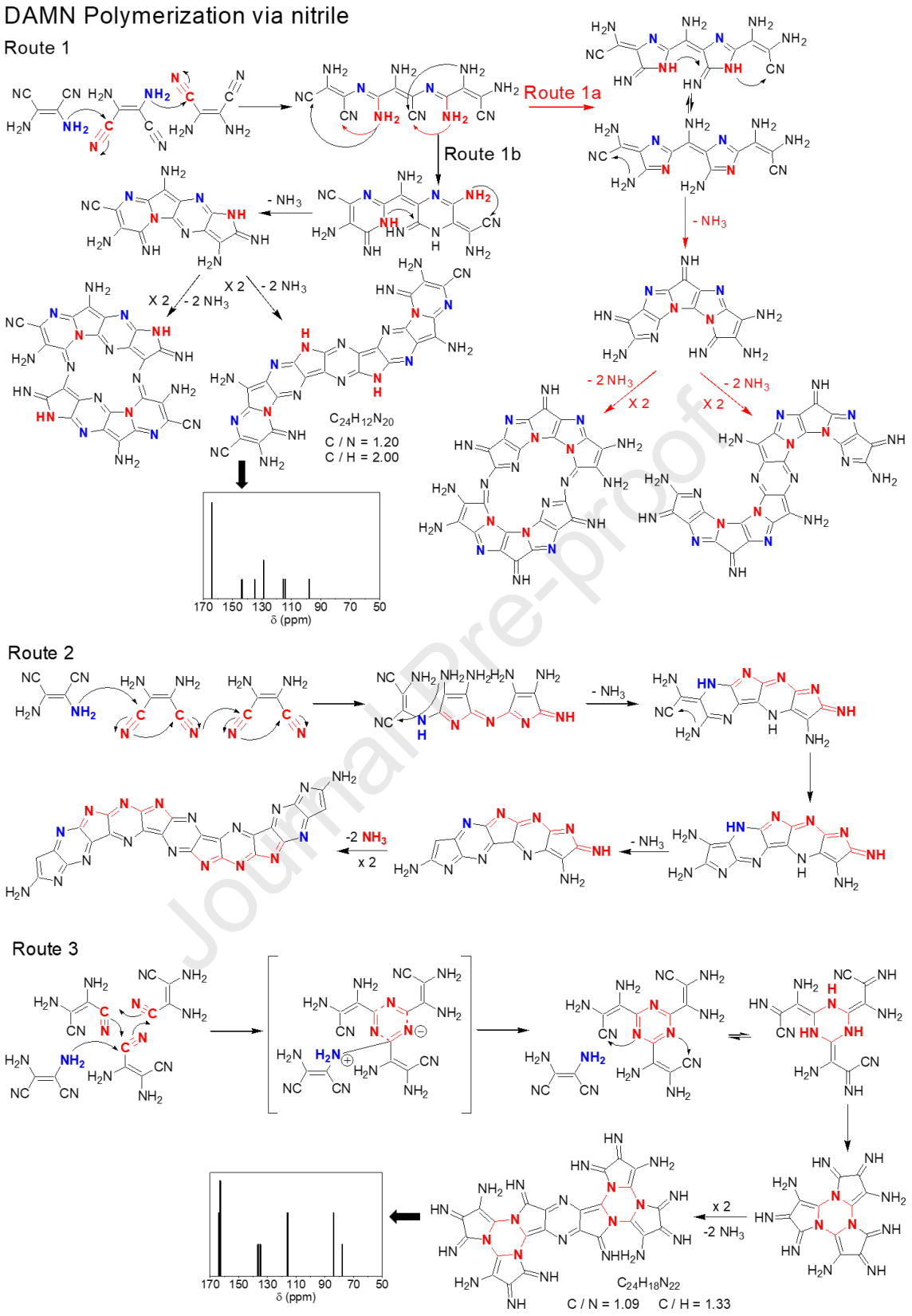


**Scheme 2**. Proposed synthetic routes with an initiation stage via nitrile for the thermoself-polymerization of DAMN.

## Conclusions

A series of layered C=N conjugated lightweight polymeric materials with relevant electromagnetic properties were prepared from DAMN with excellent product yields. These self-initiated bulk thermal polymerizations seem to be included within click chemistry according to their synthetic characteristics. The experimental conditions used, such as the reaction atmosphere and the temperature, which modulate whether the polycondensation reaction occurs in the solid-state or in the melt, are barely reflected in the microstructure. On the one hand, the polymerization temperature seems to favour heterocyclic system formation, where amine and nitrile functional groups are involved. On the other hand, the polymerization under an inert nitrogen environment also affects the crystallographic features of these functional materials in accordance with the analysis from the powder XRD patterns.

Low band gap values, below those of g-$C_3N_4$, have been obtained through both DRS spectra and electrochemical measurements; consequently, these 2-D materials could be proposed as an alternative for applications in the optoelectronic fields. In addition, their catalytic properties on AP thermal decomposition have been evaluated, showing a notable potential as a new kind of combustion activator for the development of more efficient AP-based composite propellants in aerospace propulsion. The catalytic behaviour exhibited was similar, or even better, to that presented for g-$C_3N_4$ for this singular application.

All these results place the DAMN-derived polymers as a potential subgroup within the nonconventional g-$C_3N_4$, with different dinitrogen heterocycle building blocks in their macrostructures instead of triazines, but with similar and even superior physical properties. They are produced under operational simplicity and mild conditions, which are notable advantages of the present protocol, requiring less time and temperature and the absence of a controllable atmosphere than the corresponding g-$C_3N_4$ materials. All these reasons predict a promising future for them as advanced functional polymer materials.

## CRediT authorship contribution statement

M.R.-B. data curation, formal analysis, investigation, visualization, writing – review & editing. C. H. investigation and formal analysis. M.P.G.-A. data curation, formal analysis, investigation, writing – review & editing. J.L.F. conceptualization, investigation, supervision, writing – review & editing.

## Declaration of Competing Interest

The authors declare that they have no known competing financial interests or personal relationships that could have appeared to influence the work reported in this paper.

## Acknowledgements

The authors used the facilities of the Centro de Astrobiología (CAB) and the Instituto Nacional de Técnica Aeroespacial "Esteban Terradas" (INTA). This research has been funded by grant No. PID2022-140180OB-C22 by the Spanish Ministry of Science and Innovation/State Agency of Research MCIN/AEI/ 10.13039/501100011033 and by "ERDF A way of making Europe". C.H. wants to express his gratitude to INTA for his predoctoral contract. Additionally, the authors are grateful to the M. Teresa Fernández for performing the FTIR and XRD measurements, to the Service of Electronic Spin Resonance of the Centro de Ayuda a la Investigación of the Universidad Complutense of Madrid (UCM), to the Services of Thermal Analysis and Chemical Analysis of the Instituto de Ciencias de Materiales of Madrid (ICMM, CSIC) and also to Pilar Valles for her support in the SEM analysis.

**REFERENCES**

[1] B. Tian, D. Ho, J. Qin, J. Hu, Z. Chen, D. Voiry, Q. Wang, Z. Zeng, Framework structure engineering of polymeric carbon nitrides and its recent applications, Prog. Mater. Sci. 133 (2023) 101056. https://doi.org/10.1016/j.pmatsci.2022.101056.

[2] M. Fawaz, R. Bahadur, N.P. Dharmarajan, J.H. Yang, C.I. Sathish, A.M. Sadanandan, V. Perumalsamy, G. Singh, X. Guan, P. Kumar, A. Vinu, Emerging trends of carbon nitrides and their hybrids for photo-/electro-chemical energy applications, Carbon 214 (2023) 118345. https://doi.org/10.1016/j.carbon.2023.118345.

[3] Z. Junjiang, X. Ping, L. Hailong, S.A.C. Carabineiro, Graphitic carbon nitride: synthesis, properties, and applications in catalysis, ACS Appl. Mater. Interfaces 6 (2014) 16449-16465. https://doi.org/10.1021/am502925j.

[4] Y. Zeng, X. Zhan, H. Li, X. Xiong, B. Hong, Y. Xia, Y. Ding, X. Wang, Bottom-to-Up synthesis of functional carbon nitride polymer: Design principles, controlled synthesis and applications, Eur. Polym. J. 182 (2023) 111734. https://doi.org/10.1016/j.eurpolymj.2022.111734.

[5] J. Changchao, Y. Lijun, Z. Yizhu, Z. Xia, X. Kai, X. Jingsan, L. Jian, Graphitic carbon nitride films: emerging paradigm for versatile applications, ACS Appl. Mater. Interfaces 12 (2020) 53571-53591. https://doi.org/10.1021/acsami.0c15159.

[6] T.S. Miller, A.B. Jorge, T.M. Suter, A. Sella, F. Corà, P.F. McMillan, Carbon nitrides: synthesis and characterization of a new class of functional materials, Phys. Chem. Chem. Phys. 19 (2017) 15613-15638. https://doi.org/10.1039/c7cp02711g.

[7] C. Yang, B. Wang, L. Zhang, L. Yin, X. Wang, Synthesis of layered carbonitrides from biotic molecules for photoredox transformations, Angew. Chem. Int. Ed. 56 (2017) 6627-6631. https://doi.org/10.1002/anie.201702213.

[8] I. Ciria-Ramos, N. Navascués, F. Diaw, C. Furgeaud, R. Arenal, A. Ansón-Casaos, M. Haro, E.J. Juarez-Perez, Formamidinium halide salts as precursors of carbon nitrides, Carbon 196 (2022) 1035-1046. https://doi.org/10.1016/j.carbon.2022.05.051.

[9] M. Ruiz-Bermejo, J.L. de la Fuente, J. Carretero-González, L. García-Fernández, M.R. Aguilar, A comparative study on HCN polymers synthesized by polymerization of $NH_4CN$ or diaminomaleonitrile in aqueous media: new perspectives for prebiotic chemistry and materials science, Chem. Eur. J. 25 (2019) 11437-11455. https://doi.org/10.1002/chem.201901911.

[10] I. Mas, C. Hortelano, M. Ruiz-Bermejo, J.L. de la Fuente, Highly efficient melt polymerization of diaminomaleonitrile, Eur. Polym. J. 143 (2021) 110185. https://doi.org/10.1016/j.eurpolymj.2020.110185.

[11] C. Hortelano, M. Ruiz-Bermejo, J.L. de la Fuente, Solid-state polymerization of diaminomaleonitrile: toward a new generation of conjugated functional materials, Polymer 223 (2021) 123696. https://doi.org/10.1016/j.polymer.2021.123696.

[12] M. Ruiz-Bermejo, P. García-Armada, E. Mateo-Martí, J.L. de la Fuente, HCN-derived polymer from thermally induced polymerization of diaminomaleonitrile: A non-enzymatic sensor based on prebiotic chemistry, Eur. Polym. J. 162 (2022) 110897. https://doi.org/10.1016/j.eurpolymj.2021.110897.

[13] M. Ruiz-Bermejo, P. Garcia Armada, P. Valles, J.L. de la Fuente, Semiconduction Soft Submicron Particles from the Microwave-Driven Polymerization of Diaminomaleonitrile, Polymers 14 (2022) 3460. https://doi.org/10.3390/polym14173460

[14] C. Hortelano, M. Ruiz-Bermejo, J.L. de la Fuente, Air effect on both polymerization kinetics and thermal degradation properties of novel HCN polymers based on diaminomaleonitrile, Polym. Degrad. Stab. 223 (2022) 123696. https://doi.org/10.1016/j.polymdegradstab.2022.110205.

[15] I. Mamajanov, J. Herzfeld, HCN polymers characterized by SSNMR: solid state reaction of crystalline tetramer (diaminomaleonitrile), J. Chem. Phys. 130 (2009) 134503. https://doi.org/10.1063/1.3092909.

[16] M. Zhang, X. Wang, Two dimensional conjugated polymers with enhanced optical absorption and charge separation for photocatalytic hydrogen evolution, Energy Environ. Sci. 7 (2014) 1902-1906. https://doi.org/10.1039/c3ee44189j.

[17] D.M. Johnson, S.E. Reybuck, R.G. Lawton, P.G. Rasmussen, Condensation of DAMN with conjugated aldehydes and polymerizations of the corresponding imines, Macromolecules 38 (2005) 3615-3621. https://doi.org/10.1021/ma047918l.

[18] J. Lv, H. Xiao, X. He, Z. Zhu, M. Chen, W. Yang, J. Hu, K. Zeng, G. Yang, Dicyanoimidazole thermoset derived from [2.2]paracyclophane: synthesis, curing behavior and thermal properties, Polymer 260 (2022) 125372. https://doi.org/10.1016/j.polymer.2022.125372.

[19] G. Brauer, Handbook of preparative inorganic chemistry, vol. 1, second ed., Academic Press, New York & London, 1963.

[20] I. Mas, J.L. de la Fuente, M. Ruiz-Bermejo, Temperature effect on aqueous $NH_4CN$ polymerization: relationship between kinetic behaviour and structural properties, Eur. Polym. J. 132 (2020) 109719. https://doi.org/10.1016/j.eurpolymj.2020.109719.

[21] L. Chen, Z. Shen, J. Liu, J. Liang, X. Wang, Effects of oxygen on the structural evolution of polyacrylonitrile fibers during rapid thermal treatment, RSC Adv. 10 (2020) 6356-6361. https://doi.org/10.1039/c9ra08881d.

[22] A. Fernández, M. Ruiz-Bermejo, J.L. de la Fuente, Modelling the kinetic and structural properties evolution of a versatile reaction: the aqueous HCN polymerization, Phys. Chem. Chem. Phys. 20 (2018) 17353-17366. https://doi.org/10.1039/c8cp01662c.

[23] L. Florentino-Madiedo, E. Diaz-Faes, C. Barriocanal, Relationship between gCN structure and photocatalytic water splitting efficiency, Carbon 187 (2022) 462-476. https://doi.org/10.1016/j.carbon.2021.11.030.

[24] K. Ruhland, N. Haase, A. Fischer, Detailed examination of nitrile stretching vibrations relevant for understanding the behavior of thermally treated polyacrylonitrile, J. Appl. Polym. Sci. 134 (2017) 44936. https://doi.org/10.1002/app.44936.

[25] G. Socrates, Infrared and Raman Characteristic Group Frequencies: Tables and Charts, third Ed., John Wiley & Sons, Ltd, Chichester, 2001. https://doi.org/10.1002/jrs.1238.

[26] D. Rovnyak, M. Baldus, B.A. Itin, M. Bennati, A. Stevens, R.G. Griffin, Characterization of a carbon-nitrogen network solid with NMR and High Field EPR, J. Phys. Chem. B. 104 (2000) 9817-9822. https://doi.org/10.1021/jp0004157.

[27] C. He, G. Lin, K.T. Upton, H. Imanaka , M.A. Smith, Structural investigation of HCN polymer isotopomers by solution-state multidimensional NMR, J. Phys. Chem. A. 116 (2012) 4751-4759. https://doi.org/10.1021/jp301604f.

[28] M. Ruiz-Bermejo, J.L. de la Fuente, M.R. Marín-Yaseli, The influence of reaction conditions in aqueous HCN polymerization on the polymer thermal degradation properties, J. Anal. Appl. Pyrolysis 124 (2017) 103-112. https://doi.org/10.1016/j.jaap.2017.02.015.

[29] J.L. de la Fuente, M. Ruiz-Bermejo, C. Menor-Salvan, S. Osuna-Esteban, Thermal characterization of HCN polymers by TG-MS, TG, DTA and DSC methods, Polym. Degrad. Stab. 96 (2011) 943-948. https://doi.org/10.1016/j.polymdegradstab.2011.01.033.

[30] J.L. de la Fuente, M. Ruiz-Bermejo, D. Nna-Mvondo, R.D. Minard, Further progress into the thermal characterization of HCN polymers, Polym. Degrad. Stab. 110 (2014) 241-251. https://doi.org/10.1016/j.polymdegradstab.2014.09.005.

[31] B.W. Sun, H.Y. Yu, Y.J. Yang, H.J. Li, C.Y. Zhai, D.J. Qian, M. Chen, New complete assignment of X-ray powder diffraction patterns in graphitic carbon nitride using discrete Fourier transform and direct experimental evidence, Phys. Chem. Chem. Phys. 19 (2017) 26072-26084. https://doi.org/10.1039/c7cp05242a.

[32] S. Admassie, O. Inganäs, W. Mammo, E. Perzon, M.R. Andersson, Electrochemical and optical studies of the band gaps of alternating polyfluorene copolymers, Synth. Met. 156 (2006) 614-623. https://doi.org/10.1016/j.synthmet.2006.02.013.

[33] T. Johansson, W. Mammo, M. Svensson, M.R. Andersson, O. Inganäs, Electrochemical bandgaps of substituted polythiophenes, J. Mater. Chem. 13 (2003) 1316-1323. https://doi.org/10.1039/b301403g.

[34] H. Thissen, R.A. Evans, V. Ball, Films and materials derived from aminomalononitrile, Processes, 9 (2021) 82. https://doi.org/10.3390/pr9010082.

[35] V. Ball, Antioxidant activity of films inspired by prebiotic chemistry, Mater. Lett. 285 (2021) 129050. https://doi.org/10.1016/j.matlet.2020.129050.

[36] C. Pérez-Fernández, M. Ruiz-Bermejo, S. Gálvez-Martínez, E. Mateo-Martí, An XPS study of HCN-derived films on pyrite surfaces: a prebiotic chemistry standpoint towards the development of protective coatings, RSC Adv. 11 (2021) 20109-20117. https://doi.org/10.1039/d1ra02658e.

[37] J. Jung, D.J. Menzies, H. Thissen, C.D. Easton, R.A. Evans, R. Henry, A. Deletic, D.T. McCarthy, New prebiotic chemistry inspired filter media for stormwater/greywater disinfection, J. Hazard. Mater. 378 (2019) 120749. https://doi.org/10.1016/j.jhazmat.2019.120749.

[38] X. Zhou, Y. Fang, Y. Su, C. Ge, B. Jin, Z. Li, S. Wu, Preparation and characterization of poly-hydrogen cyanide nanofibers with high visible light photocatalytic activity, Catal. Commun. 46 (2014) 197-200. https://doi.org/10.1016/j.catcom.2013.12.019.

[39] M.P. Eastman, F.S.E. Helfrich, A. Ummntsev, T.L. Porter, R. Weber, Exploring the structure of a hydrogen cyanide polymer by electron spin resonance and scanning force microscopy, Scanning, 3 (2003) 19-24. https://doi.org/10.1002/sca.4950250105.

[40] C. Perez-Fernandez, J. Vega, J.L. de la Fuente, E. Mateo-Martí, P. Valles, M. Ruiz-Bermejo, Ammonium affects the wet chemical network of HCN: feedback between

prebiotic chemistry and materials science, Phys. Chem. Chem. Phys. 25 (2023) 20473-20484. https://doi.org/10.1039/d3cp00968h.

[41] Y. Baoyun, C. Hougyi, L. Chang, A. Chongwei, W. Jingyu, Z. Yong, Efficient construction of MXene/$V_2O_5$ nanocomposites for optimizing the combustion of ammonium perchlorate-based composite solid propellants; Langmuir 39 (2023) 9162-9171. https://doi.org/10.1021/acs.langmuir.3c00940.

[42] D. Ma, X. Li, X. Wang, Y. Luo, Research development on graphitic carbon nitride and enhanced catalytic activity on ammonium perchlorate, RSC Adv. 11 (2021) 5729-5740. https://doi.org/10.1039/d0ra09079d.

[43] Q. Li, Y. He, R. Peng, Graphitic carbon nitride (g-$C_3N_4$) as a metal-free catalyst for thermal decomposition of ammonium perchlorate, RSC Adv. 5 (2015) 24507-24512. https://doi.org/10.1039/c5ra01157d.

[44] V.V. Boldyrev, Thermal decomposition of ammonium perchlorate, Thermochim. Acta 443 (2006) 1-36. https://doi.org/10.1016/j.tca.2005.11.038.

[45] Y. Ren, M. Li, H. Ye, Z. Xia, Q. Yang, G. Xie, S. Chen, S. Gao, J.Y. Lu, Copper-based energetic coordination polymers regulated by $CN^-$ and $NO_3^-$ for the combustion decomposition of ammonium perchlorate, ACS Appl. Polym. Mater. 4 (2022) 4520-4527. https://doi.org/10.1021/acsapm.2c00465.

[46] C. Hortelano, M. Ruiz-Bermejo, J.L. de la Fuente, Thermal behavior and decomposition mechanism of ammonium perchlorate in the presence of C-N conjugated polymers based on diaminomaleonitrile, J. Therm. Anal. Calorim. (2024), https://doi.org/10.1007/s10973-023-12871-1.

[47] R.L. Webb, S. Frank, W.C. Schneider, The structure of HCN tetramer, J. Am. Chem. Soc. 77 (1955) 3491-3493. https://doi.org/10.1021/ja01618a021.

[48] J. Hu, W. Yang, W. Tan, B. Liang, H. Xiao, R. Li, J. Lv, K. Zeng, G. Yang, A novel development route for cyano-based high performance thermosetting resins via the strategy of functional group design-dicyanoimidazole resins, Polymer 203 (2020) 122823. https://doi.org/10.1016/j.polymer.2020.122823.

[49] M. Ruiz-Bermejo, J.L. de la Fuente, C. Pérez-Fernández, E. Mateo-Martí, A comprehensive review of HCN-derived polymers, Processes 9 (2021) 597. https://doi.org/10.3390/pr9040597.

[50] J. Lee, A.J. Kalin, T. Yuan, M. Al-Hashimi, L. Fang, Fully conjugated ladder polymers, Chem. Sci. 8 (2017) 2503-2521. http://dx.doi.org/10.1039/c7sc00154a.

[51] Y.C. Teo, H.W.H. Lai, Y. Xia, Synthesis of ladder polymers: developments, challenges, and Opportunities, Chem. Eur. J. 23 (2017) 14101. https://doi.org/10.1002/chem.201702219.

[52] A. Herrera, A. Riaño, R. Moreno, B. Caso, Z.D. Pardo, I. Fernández, E. Sáez, D. Molero, A. Sánchez-Vázquez, R. Martínez-Alvarez, One-pot synthesis of 1,3,5-triazine derivatives via controlled cross-cyclotrimerization of nitriles: A mechanism approach, J. Org. Chem. 79 (2014), 7012-7024. https://doi.org/10.1021/jo501144v.

[53] R.E. Moser, A.R. Claggett, C.N. Matthews, Peptide formation from aminomalononitrile (HCN trimer), Tetrahedron Lett. 9 (1968) 1605-1608. https://doi.org/10.1016/s0040-4039(01)99012-4.

[54] J.P. Ferris, L.E. Orgel, Studies in prebiotic synthesis. I. Aminomalononitrile and 4-amino-5-cyanoimidazole, J. Am. Chem. Soc. 88 (1966) 3829-3831. https://doi.org/10.1021/ja00968a028.

[55] C. Hortelano, M. Ruiz-Bermejo, J.L. de la Fuente, Kinetic study of the effective thermal polymerization of a prebiotic monomer: Aminomalononitrile, Polymers 15 (2023) 486. https://doi.org/10.3390/polym15030486.

**Highlights**

DAMN polymers are proposed as an alternative to conventional carbon nitrides

These macromolecular systems present a graphitic structure based on N-heterocycles as diazines

The bulk thermal polymerizations of DAMN are easy, quick, and highly efficient

**Declaration of interests**

☐ The authors declare that they have no known competing financial interests or personal relationships that could have appeared to influence the work reported in this paper.

☒ The authors declare the following financial interests/personal relationships which may be considered as potential competing interests:

Jose L. de la Fuente and Marta Ruiz-Bermejo reports financial support was provided by Spain Ministry of Science and Innovation. Marta Ruiz-Bermejo reports financial support was provided by Spanish State Research Agency. If there are other authors, they declare that they have no known competing financial interests or personal relationships that could have appeared to influence the work reported in this paper.